Thermodynamics and Morphology of Latex Blend Films

3 AUTHORS, INCLUDING:

Jose Paulo S Farinha
University of Lisbon

84 PUBLICATIONS   **1,239** CITATIONS

Thermodynamics and Morphology of Latex Blend Films

John G. Spiro,[†,§] J. P. S. Farinha,[‡,||] and M. A. Winnik*,[§]

*Department of Chemistry, University of Toronto, 80 St. George Street,
Toronto, Ontario, Canada M5S 3H6, and Centro de Química-Física Molecular,
Instituto Superior Tecnico, 1049−001 Lisboa, Portugal*

ABSTRACT: We propose a model to describe direct nonradiative energy transfer (DET) between donors and acceptors chemically attached to the two different components of a latex blend. The model describes the case of one polymer dispersed as spheres of identical diameter in a continuous matrix of the second polymer. The segment distribution of the two polymers in the interface region is calculated taking into account the binodal compositions of the polymers in the different blend domains, the amount of each component, and the theory of the interfacial region between two polymers. The model was used to characterize the interface between poly(butyl methacrylate) (PBMA) and poly(2-ethylhexyl methacrylate) (PEHMA) domains in a binary blend, that we have examined previously (*Macromolecules* **2000**, *33*, 5863). We found a drastic dependence of the donor fluorescence survival probability curves on the Flory−Huggins χ parameter and on the PBMA:PEHMA weight ratio. Since the latter ratio is known from the experimental conditions, we were able to calculate $\chi = 0.021$ from the measurements with very low uncertainty, and infer the interface thickness between the domains in the blend as approximately 5.5 nm.

Introduction

One of the classic dilemmas in the field of water-borne coatings is how to obtain continuous and void-free films possessing good mechanical strength and durability at their end-use temperature. If the polymer particles are sufficiently soft (low glass transition temperature T_g), they will deform and become space filling as the water evaporates, but the resulting coating will be tacky to the touch and not strong enough. If the particles are hard, they will not deform to produce a coating. The traditional solution to this problem has been to add volatile organic solvents (coalescing aids) to the formulation. This plasticizes the high T_g latex polymer, lowering its modulus, and promotes film formation.[1] The film regains its desirable mechanical properties as the solvent evaporates. Unfortunately, the evaporating solvent contributes to air pollution.

With increasing concern for the environment, alternative strategies are required. One approach takes advantage of the synergistic properties of latex blends containing both hard and soft particles.[2−4] In these coatings, the hard particles provide block resistance and contribute to the strength and integrity of the film, whereas the soft particles deform to fill the voids. A number of papers[5−7] have dealt with the properties and morphologies of films cast from latex blends, particularly with aspects such as the effects of particle size, glass transition temperatures, and hard component volume fraction. These films are in many ways typical blends of immiscible polymers. They usually exhibit two glass transition temperatures, with values close to those of the individual components.[8] In these blends, some segment interpenetration occurs at the interface between the individual domains. While the volume fraction of the interfacial region is normally too small to detect by differential scanning calorimetry (DSC), it still has a large impact on the overall blend properties. Feng, Winnik, and Siemiarczuk[9] attributed the significant film stiffness at elevated temperatures in blends of hard and soft latexes to the evolution of interfaces up to 7 nm thick. Or, looking at the matter from a negative point of view, Lepizzera and co-workers[7] showed that debonding between the soft matrix and hard inclusions was responsible for loss of film integrity at high strain rates. To understand the origin of the properties of latex blends, we need a deeper understanding of the interface between the two components.

We have been interested in the use of direct nonradiative energy transfer experiments[10−15] to study interfaces in polymer blends.[16−19] In such experiments, one component is covalently labeled with one dye that can act as the donor (D), and the other component is labeled with a second dye that can act as the acceptor (A). The dyes serve as tracers for the polymer segments of the two components. Frequently, only dyes in the interfacial region are close enough for energy transfer to affect the fluorescence from the excited donor (D*). To analyze this kind of experiment, one has to combine careful donor fluorescence decay measurements with appropriate theoretical models. Two types of models are needed. One describes the rate of energy transfer in terms of the spatial distribution of donors and acceptors.[12−15] The other, from the field of polymer physics, describes the distribution of polymer segments in blends of limited miscibility.[16−19]

We recently reported a series of experiments on a hard−soft latex blend consisting of poly(butyl methacrylate) (PBMA) as the hard phase and poly(2-ethylhexyl methacrylate) (PEHMA) as the soft phase.[20] The PBMA was labeled with 1 mol % phenanthrene as the donor, and the PEHMA contained 1 mol % of anthracene groups as the acceptor. These experiments were analyzed in terms of a model that took account of the segment distribution across the interface, but led to a value of the interface thickness that was unreasonably

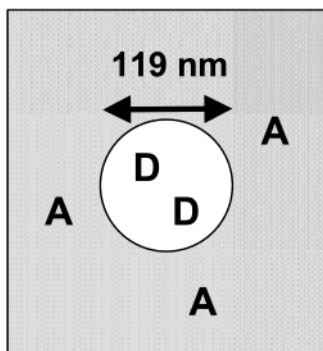* To whom correspondence may be addressed. E-mail: mwinnik@chem.utoronto.ca.
[†] E-mail: jspiro@chem.utoronto.ca.
[‡] E-mail: farinha@ist.utl.pt.
[§] University of Toronto.
[||] Instituto Superior Técnico.

Chart 1

large. A likely shortcoming of that approach was that it neglected to take account of the limited but not negligible miscibility of the two components in the blend, characterized by a thermodynamic (Flory–Huggins) χ parameter with a magnitude on the order of 0.02. In this paper, we return to these data, and reexamine them in the context of more rigorous thermodynamic theories.[19,21–25] We show that analyzing the data in this way not only leads to a better understanding of the interface thickness in these blends, but that it also provides an improved estimate of the χ parameter for PBMA–PEHMA.

The films we discuss were prepared from a 9:1 weight ratio of anthracene-labeled PEHMA and phenanthrene-labeled PBMA latex particles. Their synthesis and characterization have been described elsewhere.[26,27] On the basis of gel permeation chromatography measurements (PMMA standards), the molar masses were M_w = 56 000 and M_n = 27 000 for PEHMA and M_w = 35 000 and M_n = 17 000 for PBMA. The dye content was 1.0 mol %. The latex particles had narrow size distributions, with mean diameters of 119 nm for PBMA and 97 nm for PEHMA.

In the film newly formed at room temperature, PBMA particles were dispersed as individual spheres in a continuous PEHMA matrix. This morphology persisted upon annealing the films for an hour at 60 °C, significantly above the glass transition temperature (T_g) of both polymers. In ref 20, we modeled the system as a single PBMA particle surrounded by a PEHMA matrix. A drawing depicting this model is shown in Chart 1. Here we recognize that annealing causes changes in the system. At equilibrium the PBMA nanospheres become "saturated" with PEHMA, and the PEHMA with PBMA. The donor fluorescence decay curves that we reanalyze in this paper are the same ones presented in ref 20.

The paper is organized as follows: We begin with a description of the equilibrium thermodynamics of polymer blends, including the theory of the interfacial region between two polymers. Here, we take advantage not only of the classical formulas of Cahn, Hilliard, and de Gennes[21–23] but also of their elaboration by Anastasiadis[24] and Schubert.[25] We will then propose a specific (core–shell type) model for energy transfer calculations, describe our fluorescence simulation and analysis techniques, and show the drastic dependence of certain features of the fluorescence decay curves on the Flory–Huggins χ parameter and on the PEHMA:PBMA weight ratio. Since the latter ratio is known from the experimental conditions, we will be able to extract χ from the measurements with little uncertainty, and infer the interface thickness. We will then state our conclusions, but will also point out that they are somewhat affected

by the molecular weight *polydispersity* of each polymer in the latex blend.

Equilibrium Thermodynamics of PBMA−PEHMA Latex Blends

We begin by reviewing the theory of polymer phase separation and interface formation that is widely used to describe blends of immiscible polymers.[19] The basis of this theory, as originally proposed by de Gennes,[22,23] is the combination of Cahn and Hilliard's theory of phase separation in simple liquids and alloys[21] with the Flory–Huggins description of homogeneous polymer blends. This combination adds a *square gradient* term to the usual Flory–Huggins free energy formula, the actual terms and coefficients being derived using linear response theory within the random phase approximation.[22–24] Some details of this procedure have been reported by Anastasiadis and co-workers;[24] our computations are mostly based on their formulas. The square gradient method leads to expressions appropriate to either narrow or broad interfaces (compared to the radii of gyration of the components). The model will accommodate the intermediate case as well.[25] Some of these expressions can also be obtained from more rigorous derivations[28] or as special, limiting cases of the more rigorous models.[17]

Interfacial Profile and Interface Thickness. The basic thermodynamic relationship we have employed in our computations is the free energy formula quoted by Anastasiadis and co-workers[24] for a polymer mixture of volume V

$$G \approx \int_V [G_0(\phi) + \kappa(\nabla\phi)^2]\,dV \tag{1}$$

where $G_0(\phi)$ is the free energy density of a *uniform* system of composition ϕ (which in our blends corresponds to the PBMA volume fractions), and $\kappa(\nabla\phi)^2$ is the additional positive contribution to the free energy arising from the local concentration gradient. The parameters ϕ and κ can be given in terms of the number densities of the polymer molecules (in our case) PBMA and PEHMA (n_{PBMA} and n_{PEHMA}) and their properties: degrees of polymerization N_{PBMA} and N_{PEHMA}, specific monomer volumes u_{BMA} and u_{EHMA}, and unperturbed mean-square end-to-end distances $\langle r_0^2 \rangle_{PBMA}$ and $\langle r_0^2 \rangle_{PEHMA}$.[24]

$$\phi = \frac{n_{PBMA}N_{PBMA}u_{BMA}}{n_{PBMA}N_{PBMA}u_{BMA} + n_{PEHMA}N_{PEHMA}u_{EHMA}} \tag{2}$$

$$\frac{\kappa}{kT} = \frac{\langle r_0^2 \rangle_{PBMA}}{36\phi u_{BMA}N_{PBMA}} + \frac{\langle r_0^2 \rangle_{PEHMA}}{36(1-\phi)u_{EHMA}N_{PEHMA}} \tag{3}$$

for "broad" interfaces (relative to the radii of gyration of the polymer molecules, as mentioned above), and

$$\frac{\kappa}{kT} = \frac{\langle r_0^2 \rangle_{PBMA}}{24\phi u_{BMA}N_{PBMA}} + \frac{\langle r_0^2 \rangle_{PEHMA}}{24(1-\phi)u_{EHMA}N_{PEHMA}} \tag{4}$$

for "narrow" interfaces. In eqs 3 and 4, k is Boltzmann's constant and T is the absolute temperature. In Appendix A, we provide information on how we estimated the physical property parameters required for the computations. We have found a small Flory–Huggins

χ parameter and a correspondingly "broad" interface. Therefore, we have employed mainly eq 3 as opposed to eq 4.

We will first discuss the interfacial profile and interface thickness corresponding to a *planar* interface. The free energy formula (eq 1) then becomes[21]

$$G = \int_{-\infty}^{\infty} \{\Delta G_0[\phi(z)] + \kappa (\mathrm{d}\phi/\mathrm{d}z)^2\} \, \mathrm{d}z \qquad (5)$$

and now, in accordance with de Gennes' approach[22,23] and its implementation by Anastasiadis and co-workers,[24] we invoke the Flory−Huggins theory

$$\frac{\Delta G_0}{kT} = n_{\mathrm{PBMA}} \ln \phi + n_{\mathrm{PEHMA}} \ln(1 - \phi) + \\ \chi n_{\mathrm{PBMA}} N_{\mathrm{PBMA}} (1 - \phi) \quad (6)$$

or $\dfrac{\Delta G_0}{kT} = \dfrac{\phi}{N_{\mathrm{PBMA}} u_{\mathrm{BMA}}} \ln \phi +$

$$\frac{1 - \phi}{N_{\mathrm{PEHMA}} u_{\mathrm{EHMA}}} \ln(1 - \phi) + \frac{\chi \phi (1 - \phi)}{u_{\mathrm{BMA}}} \quad (7)$$

for unit volume (1 cm³). Equation 6 implies that χ is defined with reference to the monomeric molar volume of BMA, estimated in Appendix A. Readers will also note that we have dropped the "≈" symbol of eq 1, which was meant to indicate the approximate nature of the Cahn−Hilliard expansion.[21]

In our earlier report,[20] we neglected the mutual solubilities of PBMA and PEHMA in each other. This led to the conclusion that the interface was very broad, on the order of 25 nm for samples annealed at 60 °C. To better understand the mutual solubilities of the polymers, we now consider the critical Flory−Huggins parameter, χ_c, which separates the regions of complete ($\chi < \chi_c$) and incomplete ($\chi > \chi_c$) miscibility.

At the critical point both the second and third partial derivatives (with respect to ϕ) of the free energy function (eq 7) must vanish. The condition $\partial^3(\Delta G_0/kT)/\partial \phi^3 = 0$ yields the critical composition

$$\phi_c = \frac{[N_{\mathrm{PEHMA}} u_{\mathrm{EHMA}}/(N_{\mathrm{PBMA}} u_{\mathrm{BMA}})]^{1/2}}{1 + [N_{\mathrm{PEHMA}} u_{\mathrm{EHMA}}/(N_{\mathrm{PBMA}} u_{\mathrm{BMA}})]^{1/2}} \quad (8)$$

and substituting it into the spinodal curve equation (from $\partial^2(\Delta G_0/kT)/\partial \phi^2 = 0$), we obtain the critical χ value

$$\chi_c = \frac{u_{\mathrm{BMA}}}{2} \left[\frac{1}{(N_{\mathrm{PBMA}} u_{\mathrm{BMA}})^{1/2}} + \frac{1}{(N_{\mathrm{PEHMA}} u_{\mathrm{EHMA}})^{1/2}} \right]^2 \quad (9)$$

which in our case yields $\chi_c \approx 0.013$ (Appendix A). We also estimated that χ for our blend is not much higher than 0.02 at 60 °C. Since the system is close to the miscibility limit, we calculate the binodal compositions corresponding to given χ values and take them into consideration.

In binodal compositions, the chemical potentials of the components are equal in coexisting phases. These compositions may be determined by tangent construction to a plot of free energy of mixing vs volume fraction of PBMA (or PEHMA). We have obtained more accurate values by solving the system of nonlinear equations corresponding to the equality of chemical potentials. Details are given in Appendix B. On the basis of the data in Appendix A, we calculate the binodal composi-

Table 1. Binodal Volume Fractions of PBMA in the Core and Shell Phases (at the Annealing Temperature of 60 °C) and Corresponding Interface Thicknesses, Calculated from the Data Presented in Appendix A, and from Eqs 13 and 14

χ	0.020	0.021	0.022	0.025
δ_{calc} (nm)	5.8	5.5	5.2	4.5
ϕ_{core}	0.957 51[a]	0.966 36	0.973 21	0.986 14
ϕ_{shell}	0.099 077	0.083 887	0.071 448	0.045 351

[a] Some of our computations are sensitive to round-off errors; therefore, we report these calculated values to five significant figures.

tions in both phases (Table 1). The values in Table 1 show that the two polymers have significant miscibility, which we must account for in our calculations.

Up to now, we have followed rigorously the Cahn−Hilliard−de Gennes methods,[21−23] as elaborated by Anastasiadis and co-workers.[24] However, to determine— or even just define—the interface thickness, we must make some assumptions concerning the interfacial profile. Shifted hyperbolic tangent profiles gave good approximations to Müller and co-workers' Monte Carlo results,[18] whereas Ermoshkin and Semenov[29] employed an iterative technique, where the initial approximation was the profile

$$\phi(z) = [\phi_\alpha + \phi_\beta + (\phi_\beta - \phi_\alpha) \tanh(2z/\delta)]/2 \quad (10)$$

Here, ϕ_α and ϕ_β are the equilibrium (binodal) volume fractions of—in our case—PBMA, z is distance measured perpendicularly to the interface, and δ is the interface thickness. The latter may be defined, in the usual manner, in terms of the slope of $\phi(z)$ at $z = 0$ [$\delta = (\phi_\beta - \phi_\alpha)/(\mathrm{d}\phi/\mathrm{d}z)|_{z=0}$]. We note that eq 10 does satisfy the boundary conditions $\phi(-\infty) = \phi_\alpha$; $\phi(\infty) = \phi_\beta$; $\mathrm{d}\phi/\mathrm{d}z = 0$ at $\pm\infty$, and it seems to be a more appropriate interfacial profile for our Flory−Huggins−Cahn−Hilliard methods than those developed by Müller and co-workers[18] and Ermoshkin and Semenov[29] to suit their theoretical models.

If eq 10 is now accepted as our generic interfacial profile, determination of δ for a given χ value becomes the variational problem of minimizing the free energy given by eq 5. We can take advantage of the analogy with a particle trajectory problem in Lagrangian mechanics,[25,30] which implies that the difference between the square gradient and Flory−Huggins terms of the free energy integrand must be independent of z

$$\left[\frac{\langle r_0^2 \rangle_{\mathrm{PBMA}}}{36 \phi N_{\mathrm{PBMA}} u_{\mathrm{BMA}}} + \frac{\langle r_0^2 \rangle_{\mathrm{PEHMA}}}{36(1 - \phi) N_{\mathrm{PEHMA}} u_{\mathrm{EHMA}}} \right] \left(\frac{\mathrm{d}\phi}{\mathrm{d}z} \right)^2 - \\ \left[\frac{\phi}{N_{\mathrm{PBMA}} u_{\mathrm{BMA}}} \ln \phi + \frac{1 - \phi}{N_{\mathrm{PEHMA}} u_{\mathrm{EHMA}}} \ln(1 - \phi) + \\ \frac{\chi \phi (1 - \phi)}{u_{\mathrm{BMA}}} \right] = C \quad (11)$$

where C is the same constant for all values of z. Furthermore, because of the boundary conditions $\phi(-\infty) = \phi_\alpha$ and $\mathrm{d}\phi/\mathrm{d}z|_{z=-\infty} = 0$, the constant in question must be

$$C = -\left[\frac{\phi_\alpha}{N_{\text{PBMA}}u_{\text{BMA}}}\ln\phi_\alpha + \frac{1-\phi_\alpha}{N_{\text{PEHMA}}u_{\text{EHMA}}}\ln(1-\phi_\alpha) + \frac{\chi\phi_\alpha(1-\phi_\alpha)}{u_{\text{BMA}}}\right] \quad (12)$$

Thus, the interfacial profile must satisfy the differential equation

$$\left(\frac{\mathrm{d}\phi}{\mathrm{d}z}\right)^2 =$$

$$\frac{36}{N_{\text{PEHMA}}u_{\text{EHMA}}(1-\phi)\langle r_0^2\rangle_{\text{PBMA}} + N_{\text{PBMA}}u_{\text{BMA}}\phi\langle r_0^2\rangle_{\text{PEHMA}}} \times$$

$$\{N_{\text{PEHMA}}u_{\text{EHMA}}[\phi^2(1-\phi)\ln\phi - \phi(1-\phi)\phi_\alpha\ln\phi_\alpha] + N_{\text{PBMA}}u_{\text{BMA}}[\phi(1-\phi)^2\ln(1-\phi) - \phi(1-\phi)(1-\phi_\alpha)\times \ln(1-\phi_\alpha)] + \chi N_{\text{PBMA}}N_{\text{PEHMA}}u_{\text{EHMA}}[\phi^2(1-\phi)^2 - \phi(1-\phi)\phi_\alpha(1-\phi_\alpha)]\} \quad (13)$$

Substituting from eq 10, we see that the interface thickness will be given by the solution of the algebraic equation

$$\left(\frac{\phi_\beta - \phi_\alpha}{\delta}\right)^2 = \text{rhs} \quad \text{at } \phi = (\phi_\alpha + \phi_\beta)/2 \quad (14)$$

where rhs is the right-hand side of the differential eq 13.

In this approach, the use of eqs 5 or 13 does not guarantee that the hyperbolic tangent interfacial profile (eq 10) is the correct solution to the variational problem. Indeed, Broseta and co-workers[30] employed a more rigorous approach: numerical integration of an equation corresponding to our eq 13. However, their results, presented in graphical form and compared to the Helfand−Tagami profile[16] (rigorous for infinitely high molecular weights), confirm that our eqs 10 and 14 are good approximations. A similar conclusion can be drawn from the results described in refs 18 and 29.

Figure 1 shows the interfacial profile for a PBMA−PEHMA blend characterized by $\chi = 0.02$ and with component properties as estimated in Appendix A. From eqs 13 and 14 we obtained $\delta = 5.8$ nm, appreciably larger than the component radii of gyration; hence, eq 3 *is* the appropriate formula for the square gradient coefficient κ. However, the results shown in Figure 1 are based on the presumption that there are sufficient quantities of both PBMA and PEHMA present, so that one does not obtain a single-phase mixture. A single phase can arise because of the small but nonzero mutual solubilities of the polymers. Material balance considerations are an important part of our energy transfer model. For instance, at $\chi = 0.02$, the 9:1 PEHMA: PEHMA weight ratio would give an homogeneous mixture. We could rule out such a small value of χ a priori, because we have independent experimental evidence[31] that our latex blend films are phase separated, but our fluorescence decay data also confirm this conclusion (see the "Results and Discussion" section).

Distribution of The Blend Components

The expected morphology of an initial latex blend film containing individual PBMA nanospheres dispersed in a PEHMA matrix is shown in Chart 1. We now allow for the PBMA particles to be swollen by PEHMA and for some of the PBMA to dissolve in the PEHMA matrix,
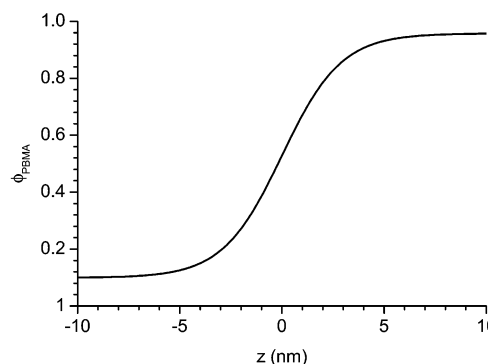

Figure 1. Calculated theoretical polymer segment density profile for a PBMA ($N_{\text{PBMA}} = 118$)/PEHMA ($N_{\text{PEHMA}} = 136$) "sandwich" (eq 10) at 60 °C, for $\chi = 0.020$. See the text.

in accordance with the binodal compositions at the annealing temperature of 60 °C (Table 1).

It will be convenient to consider the volume fraction of PEHMA in a spherical geometry

$$\psi(r) = \{\psi_\alpha + \psi_\beta + (\psi_\beta - \psi_\alpha)\tanh[2(r - R_s)/\delta]\}/2 \quad (15)$$

where ψ_α and ψ_β are the binodal volume fractions (e.g., for $\chi = 0.021$, $\psi_\alpha \approx 0.0336$ and $\psi_\beta \approx 0.916$ are the volume fractions of PEHMA in the two phases at equilibrium), δ is the interface thickness (from eqs 13 and 14), r is the distance from the center of a swollen PBMA nanosphere, and R_s is the radius of the sphere where the PEHMA concentration reaches the average of the values ψ_α and ψ_β. Before equilibration, the diameter of a PBMA nanosphere is 119 nm[20]—the diameter of the colloidal PBMA particles dispersed in water. Let us now suppose that PEHMA swells this to 130−131 nm, corresponding to all available PEHMA per PBMA particle (nine times the weight of PBMA). (We postulate volume additivity.) From a material balance and eq 15, with parameters corresponding to $\chi = 0.021$, we then find R_s to be approximately 30 nm. This value is surprisingly smaller than the radius of the original colloidal PBMA particles, and we note that in this blend the PEHMA concentration essentially reaches its equilibrium value ψ_β at $r = 40$ nm.

In other words, *from the point of view of energy transfer computations*, we cannot distinguish between swollen PBMA particles dispersed in a "contaminated" PEHMA matrix and a collection of core−shell-type superparticles, each composed of a PBMA-rich core and a corona containing mainly PEHMA (Figure 2). Note that this modeling does not imply in any way that the blends of hard and soft latexes have the same properties as core−shell latexes.

We will then search for parameters R_s and δ_{fit} (the interface thickness recovered from fitting the experimental donor fluorescence decay profiles) such that (i) R_s is compatible with the material balance (R_s depends primarily on the Flory−Huggins χ parameter and on the PEHMA:PBMA weight ratio); (ii) for a given R_s, δ_{fit} is in the best agreement with the experimental donor fluorescence decay measurements; (iii) the δ_{fit} value obtained by fitting the experimental donor fluorescence decay curves agrees closely with the theoretical interface thickness δ_{calcd}, calculated from eqs 13 and 14—a function of the Flory−Huggins χ parameter alone.

Fluorescence decay curve simulations and analyses involved in implementing the above plan will be dis-
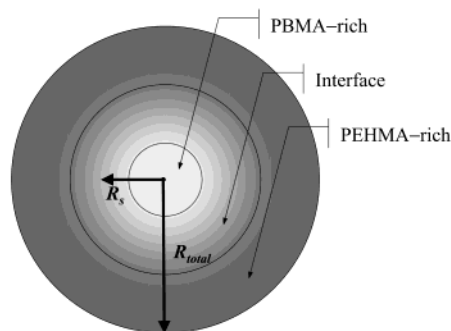
Figure 2. Model core−shell-type superparticles, each composed of a PBMA-rich core and a corona containing mainly PEHMA. The original PBMA particles are swollen by PEHMA, and some of the PBMA is dissolved in the PEHMA matrix.

cussed in the following section. Here, we would like to address the theoretical issue of whether it is justifiable to transfer the results of the variational analysis of eqs 10−14 from an unconstrained planar geometry to a core−shell model constrained by material balance restrictions and the finite mutual solubilities of the two polymers.

To our knowledge, little information has been published on the interfacial profile applicable to core−shell systems. However, Schubert[25] has shown that for core radii (which may be identified as our R_s values) considerably larger than the interface thickness (δ_{planar}), the local geometry is essentially planar. We can replace the Helfand−Tagami interfacial profile[16]

$$\psi_{HT}(z) = [1 + \tanh(2z/\delta_{planar})]/2 \quad (16)$$

by its spherical analogue[20]

$$\psi_{HT}(r) = \{1 + \tanh[(2(r - R_s)/\delta_{spherical})]\}/2 \quad (17)$$

with $\delta_{spherical}$ only very slightly larger than δ_{planar}. To introduce finite solubilities and material balance restrictions as well, but also to avoid major mathematical complexities, we will proceed as follows.

Our starting point will be the PBMA nanoparticles of diameter 119 nm.[20] The 9:1 PEHMA:PBMA weight ratio, using the component properties from Appendix A and assuming volume additivity, suggests that we can represent the latex blend as composed of particles of radius $R_{total} \approx 130.66$ nm (Figure 2). The total quantity of PEHMA contained in such a particle will be $V_{PEHMA} \approx 8.5 \times 10^6$ nm³. We can now write a material balance equation in terms of our PEHMA distribution function $\psi(r)$, eq 15, and this will also *induce a material balance* on the radial Helfand−Tagami function, eq 17

$$V_{PEHMA} = \int_0^{R_{total}} 4\pi r^2 \psi(r) \, dr =$$
$$4\pi \psi_\alpha R_{total}^3/3 + 4\pi(\psi_\beta - \psi_\alpha)\int_0^{R_{total}} r^2 \psi_{HT}(r) \, dr \quad (18)$$

For example, as we mentioned earlier, at $\chi = 0.021$ the binodal compositions are $\psi_\alpha = 0.033645$, $\psi_\beta = 0.916113$ (volume fractions of PEHMA), and our material balance becomes (approximately)

$$\int_0^{130.66} r^2 \tanh[2(r - R_s)/\delta] \, dr = 725\,750 \quad (19)$$

In Appendix C, we will conduct a free energy minimization constrained by eq 19. Employing Schubert's

Lagrange multiplier technique[25] would now be cumbersome. Instead, we will examine how, among all possible values of R_s and δ that satisfy the material balance (eq 19), we can select those that also minimize the Cahn−Hilliard free energy formula (eq 1), simplified by neglecting the combinatorial entropy terms.[25]

Similar to Schubert's conclusions regarding core−shell systems,[25] we find that neither the spherical symmetry implied by core−shell systems nor the material balance constraints applicable in our work alter δ significantly (compared to δ_{planar}) for the $\psi_{HT}(r)$ profile. It then seems reasonable to postulate that the distribution eq 15, with δ as computed from eqs 13 and 14, adequately represents our latex blend.

Energy Transfer Model

Here, we describe the model for direct nonradiative energy transfer[10−15] between two dyes attached to the components of a binary polymer blend consisting of spheres in a matrix. Since the dyes are attached at random, each to their respective polymer, the distribution of donors (phenanthrene) follows the segment distribution of the polymer to which the donor is attached (PBMA), and the distribution of acceptors (anthracene) follows the segment distribution of PEHMA. We consider all droplets to be equivalent and thus related by translational symmetry. The blend can thus be modeled as a set of identical core−shell-type superparticles consisting of PEHMA-swollen PBMA cores and shells containing PEHMA contaminated with PBMA, with an interfacial region between them (Figure 2). The compositions of the core and the shell are defined by the binodal volume fractions and are constrained by material balance. In the previous section, we described the structural model that describes the distribution of polymer segments in such a core−shell type superparticle. Here, we describe the corresponding fluorescence decay curve simulations and analyses. They are based on the fundamental principles of energy transfer kinetics and on some practical aspects of how they are applied—all of which have been discussed in ref 20.

Our starting point will be eq 20, below, identical to eq 11 of ref 20. We employ the same energy transfer rate function $w(r)$ and encounter radius R_e, as well as the same energy transfer parameters (see below). Certain approximations, such as truncating the improper integral of eq 20b at $r = 3R_0$ are also the same as in our previous publication.

$$I_D(t) = \exp\left(-\frac{t}{\tau_D}\right)\int_{V_s} C_D(r_D)\varphi(t,r_D)r_D^2 \, dr_D \quad (20a)$$

$$\varphi(t,r_D) = \exp\left(-\frac{2\pi}{r_D}\int_{R_e}^\infty\{1 - \exp[-w(r)t]\} \times \right.$$
$$\left. [\int_{|r_D - r|}^{r_D + r}C_A(r_A)r_A \, dr_A]r \, dr\right) \quad (20b)$$

where $I_D(t)$ is the fluorescence intensity, normalized to unity at zero time ($t = 0$), τ_D is the unquenched donor lifetime, and $C_D(r_D)$ and $C_A(r_A)$ are the donor and acceptor concentrations at distances r_D and r_A, respectively, from the particle center. The acceptor concentration profile must have units of number density. V_s is the volume containing the donors (in our case, the volume of the core−shell-type particle).

To analyze the experimental donor fluorescence decay profiles, we simulate donor survival probability curves
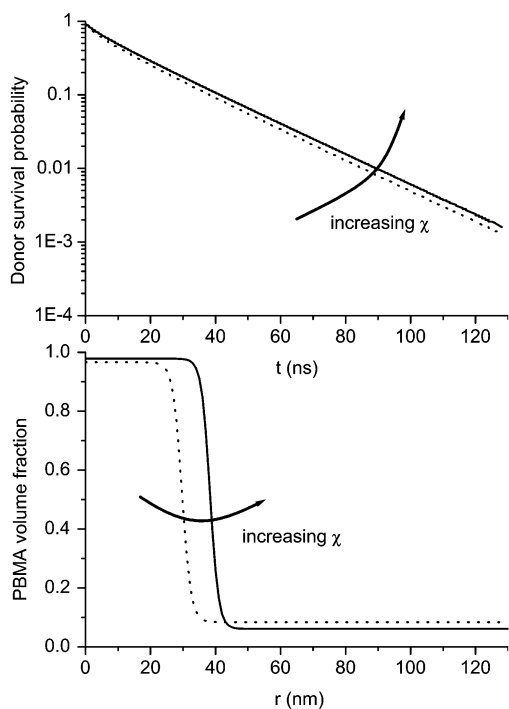
Figure 3. Simulated donor survival probability curves (top) and interfacial profiles (bottom) for $\chi = 0.021$ (···) and $\chi = 0.022$ (−).

Figure 4. Simulated donor survival probability curves for $\chi = 0.021$ (corresponding to an interface thickness of $\delta_{calcd} = 5.5$ nm) and PEHMA:PBMA weight ratios of 8:1, 9:1, and 10:1 (top). The donor distribution profiles that correspond to these curves are also shown (bottom).

according to eq 20, for trial polymer distribution functions with various R_s values, in which the interface thickness is treated as the variable parameter. All other parameters describing the system are known from calculation or from independent experiments. The distribution functions of donors and acceptors used in the calculation of the donor probability decay profiles are obtained from eq 15, considering the binodal compositions of PBMA and PEHMA in the system and their material balance.

Different donor survival probability curves were simulated, using R_s values that are compatible with the material balance. The R_s values in turn depend on the Flory–Huggins χ parameter of the blend and the PEHMA:PBMA weight ratio (through the material balance). To obtain these R_s values, we first consider different possible χ parameters. We then allow for an uncertainty of up to 10% in the PEHMA:PBMA weight ratio and select all values of R_s that are compatible with the material balance of the blend. These simulated donor survival probability curves are then compared with the experimental donor fluorescence decay profiles, allowing us to extract the interface thickness δ_{fit} that best fits the experimental results. This value is finally compared with the theoretical value of the interface thickness (δ_{calcd}), calculated from eqs 13 and 14, which is a function of the Flory–Huggins χ parameter alone.

In Figure 3 we show the effect of the Flory–Huggins χ parameter on the PBMA density profile and the donor survival probability. We simulated donor survival probability curves for $\chi = 0.021$ and $\chi = 0.022$, corresponding to interface thickness values of $\delta_{calcd} = 5.5$ and 5.2 nm, respectively. The binodal compositions of PBMA for both cases are given in Table 1. Assuming that the PEHMA:PBMA weight ratio is 9:1, we calculate values of $R_s = 29.7$ and 38.3 nm, respectively. For the higher Flory–Huggins χ parameter, the interface is only slightly
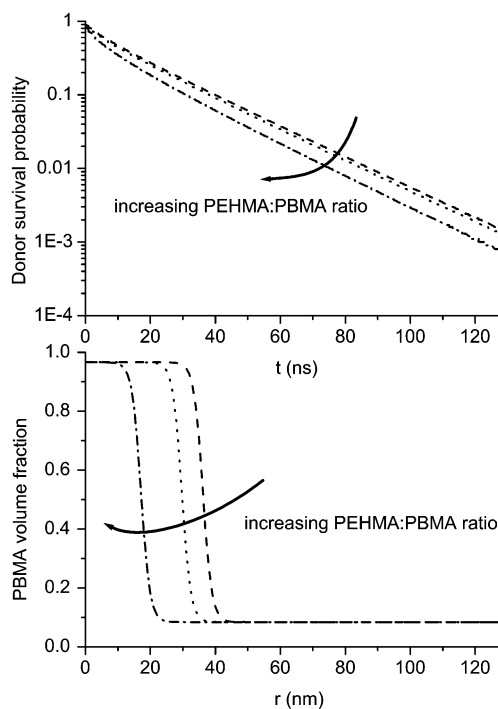
thinner, as one would expect, and the binodal compositions are also only marginally different. The stronger effect is noticed in the R_s values (Figure 3, bottom). This effect is due to the lower amount of PBMA in the PEHMA-rich phase for $\chi = 0.022$, which results in more PBMA being available for the PBMA-rich phase. The result of this slight change in the Flory–Huggins χ parameter is still noticeable in the donor survival probability (Figure 3, top). The donor survival probability decreases more slowly for the higher χ value, because in this case there is less donor-labeled PBMA in close contact with the acceptor-labeled PEHMA. In these simulations, we used $\kappa^2 = 0.478$, $R_0 = 2.3$ nm, and $\tau_D = 45.5$ ns and a cutoff distance $R_e = 0.5$ nm.[20] The initial average concentration of the acceptor in the matrix is $C^0_A = 0.05$ M.[20]

In Figure 4, we show simulated donor survival probability curves for $\chi = 0.021$ (corresponding to an interface thickness of $\delta_{calcd} = 5.5$ nm) and PEHMA:PBMA weight ratios of 8:1, 9:1, and 10:1. Material balances for these weight ratios yield equilibrated radii of $R_s = 36.2$, 29.7, and 17.1 nm, respectively. The donor distribution profiles that correspond to these curves are also shown. We used the same photophysical parameters as in Figure 3. For the higher PEHMA:PBMA weight ratio, a lower fraction of the PBMA is in the particle core (Figure 4, bottom), and more is found in the PEHMA-rich shell region. This increases the amount of energy transfer observed in the system in an easily detectable way (Figure 4, top). We thus conclude that the proposed energy transfer model can detect quite small changes in blend properties. This sensitivity is due to the strong distance dependence of energy transfer, and will allow us to characterize the blend with good precision.
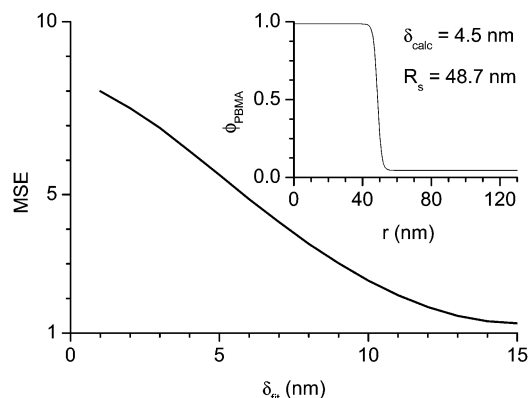
Figure 5. MSE obtained from donor survival probability curves simulated for several trial δ_{fit} values, all for $\chi = 0.025$ ($\delta_{calcd} = 4.5$ nm) and a PEHMA−PBMA weight ratio of 9:1, when fitting them to an experimental donor decay curve.

Results and Discussion

We use the equations described above to simulate donor survival probability curves and compare these curves to experimental donor fluorescence decay profiles measured for 9:1 PEHMA−PBMA blends. To compare the experimental and simulated curves, the noise-free simulated donor survival probability curves $I_D(t)$ obtained using eq 20 were convoluted with experimental instrument response functions $L(t)$, obtained from the excitation source, as described previously.[32] We refer to the simulated decays convoluted with real lamp excitation profiles as $I_D^{conv}(t)$.

$$I_D^{conv}(t) = \int_0^t L(s) I_D(t - s) \, ds \qquad (21)$$

Comparison of the experimental and simulated decays is done by least-squares fit

$$I_D^{exp}(t) = a_N I_D^{conv}(t) + a_L L(t) \qquad (22)$$

where the only fitting parameters are the normalization factor of the decay intensity a_N, and the light-scattering correction a_L.[33] This is a weighted regression, which takes into account the Poisson error of counting in the usual manner.[34] To evaluate the quality of the fitting results, we calculate the mean square error of the weighted regression (MSE)[35] and plot the weighted residuals and autocorrelation of (weighted) residuals. For simulated decays that produce acceptable fitting results (MSE close to 1, with randomly distributed weighted residuals and autocorrelation of residuals), the decay intensity normalization and light-scattering correction parameters, a_N and a_L (eq 22), do not change significantly as we explore different $I_D^{conv}(t)$ functions.

Previous results suggest that at 60 °C the Flory−Huggins χ parameter for our blend is not much higher than 0.02.[20] To place an upper bound on the possible Flory−Huggins χ parameters of our blend, we first consider $\chi = 0.025$. Using eqs 13 and 14, we calculate the corresponding theoretical interface thickness, $\delta_{calcd} = 4.5$ nm. For a PEHMA−PBMA weight ratio of 9:1, the material balance leads to $R_s = 48.7$ nm. Using the parameters[20] $\kappa^2 = 0.478$, $R_0 = 2.3$ nm, $\tau_D = 45.5$ ns, $R_e = 0.5$ nm, and $C^0_A = 0.05$ M, we simulate donor survival probability curves for several trial δ_{fit} values, from 1 to 15 nm. In Figure 5, we show the MSE resulting from fitting simulated curves to an experimental donor decay.
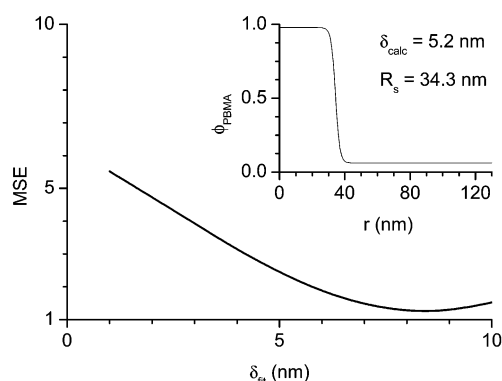

Figure 6. MSE obtained from fitting donor survival probability curves simulated for several trial δ_{fit} values, all for $\chi = 0.022$ ($\delta_{calcd} = 5.2$ nm) and a PEHMA−PBMA weight ratio of 9.9:1, to an experimental donor decay curve. The interface profile and thickness obtained from thermodynamic calculations are shown in the inset.

Even at a very large interface thickness of 15 nm (far from $\delta_{calcd} = 4.5$ nm; Figure 5 inset), a good fit could not be obtained—the MSE is high and the distributions of weighted residuals and the autocorrelation of residuals are skewed. For lower δ values, the fitting results were even worse. We therefore conclude that $\chi = 0.025$ is not compatible with our experimental results. (The value $\delta_{calcd} = 4.5$ nm may be imprecise, because the "broad" interface formula eq 3 may not be entirely appropriate here, but this has little bearing on our conclusion.)

We now consider $\chi = 0.022$ (corresponding to $\delta_{calcd} = 5.2$ nm), and simulate donor survival probability curves for different PEHMA−PBMA weight ratios and several trial δ_{fit} values. Using PEHMA:PBMA = 9:1, we obtained a fitting result similar to the case where we had $\chi = 0.025$: a thick interface. If we allow for a PEHMA: PBMA weight ratio variation of about 10% relative to the 9:1 expected value, we now obtain better fitting results. From the results in Figure 6 (PEHMA:PBMA = 9.9:1, giving $R_s = 34.3$ nm, as in the inset), we conclude that the best fitting of simulated curves to the experimental donor decay is achieved for approximately $\delta_{fit} = 8.0$ nm. Although the fitting itself is acceptable, the interface thickness obtained is far too different from the theoretical interface thickness (Figure 6 inset) calculated for $\chi = 0.022$. Consequently, we must discard this result and try a still lower χ value.

At $\chi = 0.021$, the calculated interface thickness is $\delta_{calcd} = 5.5$ nm. Using the corresponding PBMA binodal volume fractions (Table 1) we calculate equilibrated R_s values for five different PEHMA−PBMA weight ratios, ranging from 9:1 to 10:1 ($R_s = 30-17$ nm), and simulate donor decay curves for these conditions. We then fit these curves to the experimental decay curves and again evaluate the fitting results by calculating the MSE, the weighted residuals, and autocorrelation of the residuals. With this rough grid mapping procedure, we identify the best-fitting δ_{fit} values for each R_s (Figure 7, top). By comparing these values to the interface thickness calculated from the Flory−Huggins χ parameter ($\delta_{calcd} = 5.5$ nm), we are able to pinpoint the weight ratio region where the fitted interface thickness agrees with the theoretical value. From the result shown in Figure 7, bottom, we conclude that our region of interest lies around $R_s = 26$ nm (corresponding to a PEHMA:PBMA weight ratio of 9.4:1, well inside the 10% uncertainty
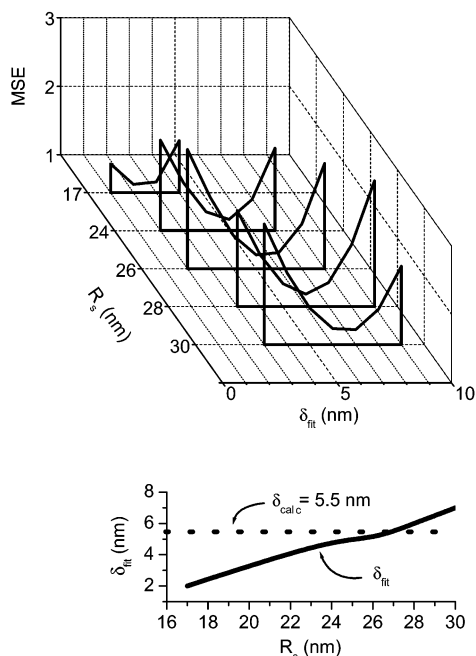
Figure 7. Examination of the effect of assumed PEHMA:
PBMA weight ratios and corresponding R_s values at $\chi = 0.021$
on predicted values (δ_{fit}) of the interface thickness (top).
Selection of the region of interest (bottom).

Figure 8. Experimental instrument response function and
experimental donor decay profile obtained for a PEHMA−
PBMA blend, annealed for 1 h at 60 °C. Examination was
performed of corresponding simulated results and autocorre-
lation plots for $\chi = 0.021$ and different trial interface thick-
nesses.

Figure 9. Fine search over the trial interface thicknesses δ_{fit}
when fitting an experimental donor decay profile obtained for
a PEHMA−PBMA blend, annealed for 1 h at 60 °C. Donor
survival probability curves were simulated with $\chi = 0.021$
($\delta_{calcd} = 5.5$ nm, $R_s = 26$ nm, see the inset).

interval of the 9:1 experimental value that we consider
in order to account for a small amount of agglomeration
of PBMA particles observed[31] at the film edges by laser
scanning fluorescence confocal microscopy).

Let us take a closer look now at fitting the experi-
mental donor decay with curves simulated for $R_s = 26$
nm and different δ_{fit} values. In Figure 8, we show an
experimental decay obtained for our blend, the corre-
sponding instrument response function, and simulated
donor survival probabilities for different trial interface
thickness values: $\delta_{fit} = 2.0$, 5.5, and 8.0 nm. Although
the three simulated curves are apparently similar, their
fitting to the experimental donor decay curve produced
very different results. For $\delta_{fit} = 2.0$ nm and $\delta_{fit} = 8.0$
nm the autocorrelation functions (Figure 8 inset) are
clearly nonrandomly distributed, indicating that the
simulated curves cannot describe the experimental
result. In contrast, with $\delta_{fit} = 5.5$ nm we obtain a well-
distributed autocorrelation plot of the weighted residu-
als.

To better define the error bar for the fitted interface
width, we conducted a fine search around $\delta_{fit} = 5.5$ nm
and determined the interval of δ_{fit} for which the auto-
correlations of the residuals are randomly distributed.
From a similar analysis as the one shown in Figure 8,
we found that an acceptable autocorrelation distribution
is obtained for approximately $\delta_{fit} = 5.0-6.0$ nm. The
flatness of the MSE plot obtained for this interval of
δ_{fit} values (Figure 9) led us to accept the value $\delta_{fit} = 5.5$
± 0.5 nm.

At this point we had found a set of parameters $\delta_{fit} =
5.5 \pm 0.5$ nm and PEHMA:PBMA weight ratio of 9.4:1
(corresponding to $R_s = 26$ nm) that satisfy the con-
straints we set out in the section Distribution of the
Blend Components. The R_s value is compatible with the
material balance for $\chi = 0.021$; it corresponds to a
PEHMA:PBMA weight ratio of 9.4:1. The interface
thickness $\delta_{fit} = (5.5 \pm 0.5)$ nm agrees well not only with
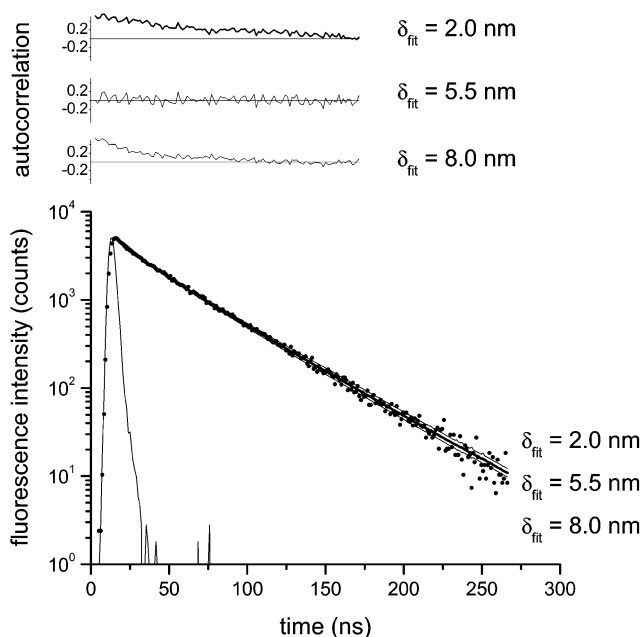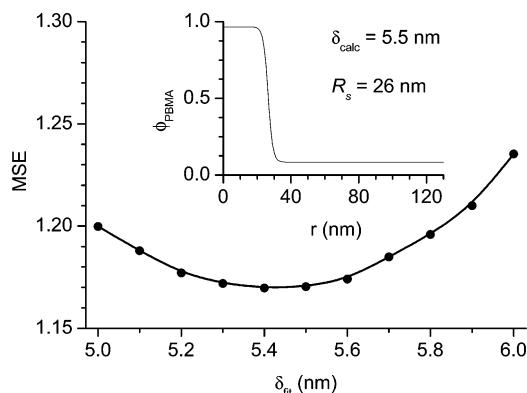the experimental fluorescence donor decay curves but

also with the theoretical interface thickness $\delta_{calcd} = 5.5$
nm calculated from eqs 13 and 14 for a Flory−Huggins
parameter of $\chi = 0.021$.

We have seen before that it was impossible to meet
these conditions for χ parameters higher (by 0.001 or
more) than $\chi = 0.021$. However, to accept the value $\chi =
0.021$ for the Flory−Huggins parameter, we still have
to examine χ parameters lower than this value.

Let us now consider $\chi = 0.020$, for which we obtain
$\delta_{calcd} = 5.8$ nm. For a weight ratio PEHMA:PBMA =
9:1, the binodal compositions (Table 1) and material
balance calculations imply that the blend should be
miscible. We should obtain an homogeneous distribution
of donors and acceptors, and the donor fluorescence
decay should conform to the Förster model

$$I_D(t) = \exp\left(-\frac{t}{\tau_D}\right) \exp\left[-P\left(\frac{t}{\tau_D}\right)^{0.5}\right] \quad (23)$$
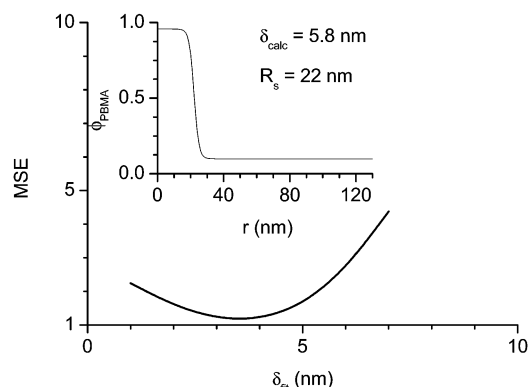
Figure 10. Rejection of $\chi = 0.020$. Even at a reduced (8.1:1) PEHMA:PBMA weight ratio ($R_s = 22$ nm, see the inset), the interface thickness obtained is unacceptable. Cf. Figure 6.

where the parameter P depends on the local concentration of acceptors and on the averaged relative orientation κ^2 of the donor and acceptor transition moments.[10,11,20]

The experimental donor decay curve can indeed be approximately described by the Förster model ($P = 0.385$ for a fixed donor lifetime $\tau_D = 45.5$ ns), with MSE $= 1.3$ and a randomly distributed autocorrelation of weighted residuals. However, if we calculate P from the acceptor concentration in the blend assuming complete mixing between the polymers,[20] we obtain $P_{mix} = 2.086$. The large difference between the calculated and fitted P values is not only inconsistent with a single-phase system, but it also tells us that the donors in the blend are "seeing" a much smaller number of acceptors than they would in a miscible system. Therefore, even at 60 °C, our results rule out a single-phase system. This is in agreement with laser scanning confocal fluorescence microcopy results obtained for the same blend.[31]

To match the energy transfer efficiency of the experimental donor fluorescence decays while considering $\chi = 0.020$, we would have to allow for very low PEHMA– PBMA weight ratios. If we consider the lowest value within the 10% confidence interval around the experimental PEHMA:PBMA weight ratio (PEHMA:PBMA = 8.1:1), we obtain an immiscible system with approximately $R_s = 22$ nm. For these conditions, we simulated donor survival probability curves and tried to match the experimental donor decay curve (Figure 10). The best fit was obtained for approximately $\delta_{fit} = 3.0–4.0$ nm. Again, the quality of the fitting is acceptable but the interface thickness obtained is far form the theoretical interface thickness $\delta_{calcd} = 5.8$ nm calculated for $\chi = 0.020$ (Figure 10 inset). At $\delta_{fit} = 5–6$ nm, the fitting to the experimental decay yields MSE > 2 and biased autocorrelation of the residuals.

In conclusion, assumed Flory–Huggins χ parameters as low as (or lower than) $\chi = 0.020$ and as high as (or higher than) $\chi = 0.022$ appear to be in conflict with our data and the relevant thermodynamic theory. Therefore, we suggest 0.021 for the Flory–Huggins χ parameter of our PBMA–PEHMA latex blend at 60 °C.

It is of interest to compare our result to interactions between other polymer pairs, for instance, to tabulated data that were obtained by analyzing the phase behavior of polymer blends.[36] Since χ parameters tend to be defined in terms of different reference volumes (in our case the monomeric volume u_{BMA}), let us replace the enthalpy term $\chi\phi(1 - \phi)/u_{BMA}$ (for unit volume) of eq 7 by the equivalent[37] term B/RT, where B is the interac-

tion energy density for a monomer unit pair (in our case BMA and EHMA) and R is the gas constant. (We note that the "reference volume" for B is simply 1 cm³.) We obtain $B = 0.10$ cal/cm³, showing a much smaller degree of incompatibility than most monomer pairs listed in Table 1 of ref 36. Our result is also consistent with the small difference between the solubility parameters of PBMA and PEHMA.[38]

Summary and Conclusions

We examined a blend of two methacrylate polymers, in which the minor component, PBMA, is present as spheres of uniform size dispersed in a continuous PEHMA matrix. Both polymers were labeled with fluorescent dyes: PBMA with phenanthrene (Phe) and PEHMA with anthracene (An), suitable for direct nonradiative energy transfer (DET) experiments. The blends were prepared by mixing aqueous dispersions of the polymers in the form of latex nanospheres, casting a film, and allowing the water to evaporate. Upon drying, the soft PEHMA particles ($T_g \approx -10$ °C) in the blend deform and pack to form a continuous matrix. The PBMA particles retain their spherical shape, even after the film is annealed at 60 °C. By choosing a PEHMA: PBMA weight ratio of 9:1, corresponding to 14 PEHMA particles (diameter 97 nm) per PBMA particle (diameter 119 nm), we ensured that each donor-labeled PBMA droplet in the blend was surrounded by the acceptor-labeled matrix.[20]

We carried out DET experiments and developed a model to describe energy transfer between donors and acceptors chemically attached to the two different components of the polymer blend. The model describes the case of one polymer dispersed as spheres of identical diameter in a continuous matrix of the second polymer. This model takes explicit account of the segment distribution of the two polymers in the interface region, based on the equilibrium thermodynamics of the blend and on the theory of the interfacial region between two polymers. We found a drastic dependence of the donor survival probability curves on the Flory–Huggins χ parameter and on the PBMA:PEHMA weight ratio. Since the latter ratio is known from the experimental conditions, we were able to calculate $\chi = 0.021$ from the measurements with very low uncertainty, and infer that the interface thickness between the domains in the blend is approximately $\delta = 5.5$ nm. This result corresponds to an interaction energy density[36,37] of $B = 0.10$ cal/cm³.

Direct nonradiative energy transfer (DET) experiments provide a useful and powerful method to determine both the Flory–Huggins χ parameter of two polymers in a blend and the thickness of the interface between the adjacent polymer phases. The method can in principle be applied to any system in which the dispersed phase can be prepared in the form of uniform spheres. The equations used to describe the distribution of polymer segments are good approximations for spherical geometry and account for the polymer binodal compositions in the different blend domains.

Our fluorescence decay curves are such sensitive functions of χ because the solubilities of PBMA and PEHMA in each other are significant. From a theoretical perspective, combining the binodal compositions with the material balance has a drastic effect on the morphology. For instance, if we assume $\chi = 0.020$ for our 9:1 weight ratio PEHMA:PBMA blends, the binodal

compositions would be $\phi_\alpha = 0.0991$ and $\phi_\beta = 0.9575$ (volume fractions of PBMA), and we would predict that the blend consists of a single phase after equilibration. On the other hand, at $\chi = 0.022$, the mutual solubilities of PBMA and PEHMA are already significantly lower (PBMA volume fractions of $\phi_\alpha = 0.0714$ and $\phi_\beta = 0.9732$), so that to account for the appreciable level of energy transfer we have to postulate a much broader interface than the theoretical δ value for this χ (eqs 13 and 14).

As a matter of fact, to obtain perfect or near-perfect agreement with the theoretical prediction of δ even at $\chi = 0.021$, we had to decrease the core size R_s in the simulations from 30 to 26 nm, which corresponds to increasing the assumed PEHMA:PBMA weight ratio by 4.5% (from 9:1 to 9.4:1). This change in the assumed PEHMA:PBMA weight ratio can be justified by the fact that images taken by laser scanning fluorescence confocal microscopy show evidence of a small but detectable amount of PBMA agglomeration at the film edges, which decreases the amount of PBMA available throughout the film and leads to a higher effective PEHMA:PBMA weight ratio. Somewhat arbitrarily, we defined the criterion of acceptability for a postulated χ value as being able to recover the theoretical δ without adjusting the assumed PEHMA:PBMA weight ratio by more than 10%. In any case, even such considerable adjustments were insufficient to obtain acceptable results with $\chi = 0.020$ or $\chi = 0.022$.

Probably the weakest point of our derivations and analyses is that we estimated the properties of PBMA and PEHMA as if our samples had been monodisperse (with respect to their molecular weight). Polydispersity will also impinge on the phase equilibrium and interfacial profile relationships. We plan to discuss these matters in a forthcoming paper.

Appendix A

The physical property parameters that we required for our computations were the degrees of polymerization, molar volumes, and radii of gyration (or, equivalently, mean-square end-to-end distances) for PBMA and PEHMA. For the degree of polymerization, we treated our polymer components as if they were monodisperse. We chose values ($N_{PBMA} = 118$ and $N_{PEHMA} = 136$) based on the number-average molecular weights of 16 700 for PBMA and 27 000 for PEHMA,[20] using the respective monomer molecular weights of 142.20 and 198.31.[39] From Olabisi and Simha's experimental data,[40] the specific volume of PBMA is 0.9694 cm³/g at 60 °C. To obtain the specific volume of PEHMA, we have employed a group contribution method,[41] as well as Simha and Boyer's correlation.[42] The glass transition temperature of PEHMA, needed for the calculations, was taken to be 263 K.[43]

The group contribution calculation[41] yielded a PEHMA specific monomer volume[24] of 200.41 cm³/mol at 25 °C. This value was adjusted to 204.83 cm³/mol at 60 °C, using Simha and Boyer's relationship $\alpha_L T_g = 0.164$,[42] where α_L is the coefficient of (cubic) thermal expansion above the glass transition temperature T_g (K). The specific monomer volume of PBMA is $0.9694 \times 142.20 = 137.85$ cm³/mol at 60 °C.

Estimation of the radii of gyration of PBMA and PEHMA was a less straightforward matter. For instance, the latest edition of the *Polymer Handbook*[44] mentions more recent work that challenges earlier[44,45] data on PBMA. However, those more recent results were obtained on ultrahigh molecular weight samples of higher polydispersity, prepared by plasma-induced polymerization, and may not be relevant to our work. We have decided to rely on an earlier formula, also adopted by Helfand and Sapse in their well-known tabulation[46] of statistical segment lengths: $r_0/M^{1/2} = 0.051$ nm for PBMA at 23 °C. Here, r_0 is the square root of the unperturbed mean-square end-to-end distance, and M is the molecular weight. To correct r_0 (for PBMA) to the annealing temperature of 60 °C, we also employed the *Polymer Handbook* datum[44] for thermal expansion: $d(\ln r_0^2)/dT = 2.5 \times 10^{-3}$ deg⁻¹. This resulted in the mean-square end-to-end distance 47.87 nm² at 60 °C for our PBMA sample of $M_n = 16\,700$. We note that the $r_0/M^{1/2} = 0.051$ nm formula applies to poly(2-ethylbutyl methacrylate) as well,[44] essentially at the same temperature (25 °C) as quoted for PBMA. It appears that for methacrylates, 2-ethyl substitution in the ester groups affects the radius of gyration *only through the monomer molecular weight.* Thus, we adopted the poly(hexyl methacrylate) formula $r_0/M^{1/2} = 0.053$ nm at 30 °C, with thermal expansion $d(\ln r_0^2)/dT = 2.2 \times 10^{-3}$ (deg⁻¹), for PEHMA as well.[44] This yielded a mean-square end-to-end distance of 80.93 nm² at 60 °C for our PEHMA component of $M_n = 27\,000$.

Appendix B

From eq 6 the chemical potentials are given by

$$\frac{\Delta\mu_{PBMA}}{kT} =$$
$$\ln\phi + (1-\phi)\left(1 - \frac{N_{PBMA}u_{BMA}}{N_{PEHMA}u_{EHMA}}\right) + \chi N_{PBMA}(1-\phi)^2 \tag{B1}$$

and

$$\frac{\Delta\mu_{PEHMA}}{kT} =$$
$$\ln(1-\phi) + \phi\left(1 - \frac{N_{PEHMA}u_{EHMA}}{N_{PBMA}u_{BMA}}\right) + \chi N_{PEHMA}\frac{u_{EHMA}}{u_{BMA}}\phi^2 \tag{B2}$$

Equality of the chemical potentials then corresponds to the solution of the (nonlinear) system of equations

$$\ln\phi_\alpha - \ln\phi_\beta = \chi N_{PBMA}[(1-\phi_\beta)^2 - (1-\phi_\alpha)^2] - (\phi_\beta - \phi_\alpha)\left(1 - \frac{N_{PBMA}u_{BMA}}{N_{PEHMA}u_{EHMA}}\right) \tag{B3}$$

$$\ln(1-\phi_\alpha) - \ln(1-\phi_\beta) = (\phi_\beta - \phi_\alpha) \times \left(1 - \frac{N_{PEHMA}u_{EHMA}}{N_{PBMA}u_{BMA}}\right) + \chi N_{PEHMA}\frac{u_{EHMA}}{u_{BMA}}(\phi_\beta^2 - \phi_\alpha^2)$$

where ϕ_α and ϕ_β are the binodal compositions, given as volume fraction PBMA. Precise solutions were obtained—for various assumed χ values—with the aid of the Numerical Algorithms Group (NAG) routine C05PBF.[47]

Appendix C

We provide a partial confirmation here that our interfacial profile (eq 15) and its interface thickness

parameter δ, which are based on eq 10 (planar interface), are not invalidated by the material balance constraints that play an important part in our model. In this we follow in Schubert's[25] footsteps; he showed that the transition from planar to cubic symmetry had little effect on δ in most situations.

Our starting point is the expanded form (cf. eqs 3 and 6) of the free energy formula (eq 1):

$$\frac{G}{kT} = \int_V \left\{ n_{\text{PBMA}} \ln \phi + n_{\text{PEHMA}} \ln(1 - \phi) + \right.$$

$$\chi n_{\text{PBMA}} N_{\text{PBMA}} (1 - \phi) + \left[\frac{\langle r_0^2 \rangle_{\text{PBMA}}}{36 \phi u_{\text{BMA}} N_{\text{PBMA}}} + \right.$$

$$\left. \left. \frac{\langle r_0^2 \rangle_{\text{PEHMA}}}{36(1 - \phi) u_{\text{EHMA}} N_{\text{PEHMA}}} \right] (\nabla \phi)^2 \right\} dV \quad \text{(C1)}$$

We neglect the combinatorial entropy (first two terms of the integrand), replace $n_{\text{PBMA}} N_{\text{PBMA}}$ by $\phi_{\text{PBMA}}/u_{\text{BMA}}$ (1 cm^3 volume), introduce spherical symmetry, and approximate $\langle r_0^2 \rangle_{\text{PBMA}}/(u_{\text{BMA}} N_{\text{PBMA}}) \approx 2.9429 \times 10^{-17}$ mol cm^{-1} and $\langle r_0^2 \rangle_{\text{PEHMA}}/(u_{\text{EHMA}} N_{\text{PEHMA}}) \approx 2.9052 \times 10^{-17}$ mol cm^{-1} (Appendix A) by their mean value, which we denote by b^2/u_{BMA} (b is the effective statistical segment length). Thus, the free energy expression to be minimized, subject to the constraint eq 19, becomes

$$M = \int_0^\infty r^2 \left[\chi \phi(1 - \phi) + \frac{b^2}{36 \phi(1 - \phi)} \left(\frac{d\phi}{dr} \right)^2 \right] dr \quad \text{(C2)}$$

and substituting the radial Helfand–Tagami distribution (eq 17) for ϕ

$$M = \int_0^\infty r^2 \left[\frac{\chi}{4} + \frac{b^2}{9\delta^2} \right] \{1 - \tanh^2[2(r - R_s)/\delta]\} \, dr \quad \text{(C3)}$$

Now, we employ Schubert's approximation of extending the lower limit of integration in eq C3 from 0 to $-\infty$,[25] and introduce the transformation $z = 2(r - R_s)/\delta$, obtaining

$$M = \int_{-\infty}^\infty \left(\frac{z\delta}{2} + R_s \right)^2 \left[\frac{\chi\delta}{8} + \frac{b^2}{18\delta} \right] (1 - \tanh^2 z) \, dz \quad \text{(C4)}$$

The quadrature formulas

$$\int_0^\infty (1 - \tanh^2 z) \, dz = 1 \quad \text{(C5)}$$

and

$$\int_0^\infty z^2 (1 - \tanh^2 z) \, dz = \frac{\pi^2}{12} \quad \text{(C6)}$$

yield

$$M = \left(\frac{\pi^2 \delta^2}{48} + R_s^2 \right) \left(\frac{\chi\delta}{4} + \frac{b^2}{9\delta} \right) \quad \text{(C7)}$$

To proceed with the constrained minimization, we now have to examine the implications of eq 19. Numerical integrations for various values of R_s and δ have shown that, at least for reasonable magnitudes of δ, the integral of eq 19 is quite insensitive to δ, but very sensitive to R_s. Actually, it is difficult to establish R_s with good accuracy without fitting fluorescence decay data, because the material balance eq 19 *itself* is very

dependent on small experimental uncertainties in PBMA particle size (before equilibration) and the PEHMA: PBMA weight ratio. Nevertheless, in minimizing M (eq C7) it is reasonable to assume that R_s will be essentially constant in this process, and that even for quite large values of δ, the $\pi^2 \delta^2/48$ term is entirely negligible compared to R_s^2. Thus, free energy minimization amounts to minimizing the equation

$$M' = \chi\delta/4 + b^2/(9\delta) \quad \text{(C8)}$$

This yields

$$\delta = \frac{2b}{\sqrt{9\chi}} \quad \text{(C9a)}$$

for broad interfaces, and *mutatis mutandi*

$$\delta = \frac{2b}{\sqrt{6\chi}} \quad \text{(C9b)}$$

for narrow interfaces. These are identical to the usual formulas for the interface thickness between immiscible polymers.[25] We conclude that for large R_s/δ ratios, neither the spherical symmetry implied by core–shell-type systems, nor the material balance constraints applicable here, have a significant influence on δ, compared to a planar geometry, for the Helfand–Tagami components of our distributions. It now seems reasonable to postulate that the *complete* distribution function (eq 15), *subject to the same material balance constraint,* is appropriate for our system.

References and Notes

(1) (a) Karsa, D. R. *Additives for Water-Based Coatings*; Royal Chemical Society: London, 1990. (b) Winnik, M. A.; Wang, Y.; Haley, F. *J. Coat. Technol.* **1992**, *64*, 51.
(2) Friel, J. European Patent Application 0 466 409 A1, 1992.
(3) Feng, J.; Winnik, M. A.; Shivers, R.; Clubb, B. *Macromolecules* **1995**, *28*, 7671.
(4) Winnik, M. A.; Feng, J. *J. Coat. Technol.* **1996**, *68*, 39.
(5) Eckersley, S. T.; Helmer, B. J. *J. Coat. Technol.* **1997**, *69*, 97.
(6) Keddie, J. L.; Meredith, P.; Jones, R. A. L.; Donald, A. M. *Langmuir* **1996**, *12*, 3793.
(7) Lepizzera, S.; Lhommeau, C.; Dilger, G.; Pith, T.; Lambla, M. *J. Polym. Sci., B: Polym. Phys.* **1997**, *35*, 2093.
(8) Krause, S. In *Polymer Blends*; Paul, D. R., Newman, S., Eds.; Academic Press: San Diego, CA, 1978; Vol. I, pp 15–113.
(9) Feng, J.; Winnik, M. A.; Siemiarczuk, A. *J. Polym. Sci., Part B: Polym. Phys.* **1998**, *36*, 1115.
(10) Förster, Th. *Ann. Phys. (Leipzig)* **1948**, *2*, 55.
(11) Förster, Th. *Z. Naturforsch.* **1949**, *4a*, 321.
(12) Blumen, A.; Klafter, J.; Zumofen, G. *J. Chem. Phys.* **1986**, *84*, 1397.
(13) Farinha, J. P. S.; Martinho, J. M. G.; Yekta, A.; Winnik, M. A. *Macromolecules* **1995**, *28*, 6084.
(14) Farinha, J. P. S.; Martinho, J. M. G.; Kawaguchi, S.; Yekta, A.; Winnik, M. A. *J. Phys. Chem.* **1996**, *100*, 12552.
(15) Yekta, A.; Winnik, M. A. In *Solvents and Self-Organization of Polymers*; Webber, S. E., Munk, P., Tuzar, Z., Eds.; Kluwer: Dordrecht, The Netherlands, 1996; pp 433–455.
(16) Helfand, E.; Tagami, Y. *J. Chem. Phys.* **1972**, *56*, 3592.
(17) Fredrickson, G. H. In *Physics of Polymer Surfaces and Interfaces*; Sanchez, I. C., Fitzpatrick, L. E., Eds.; Butterworth-Heinemann: Oxford, U.K., 1992; Chapter 1.
(18) Müller, M.; Binder, K.; Oed, W. *J Chem. Soc., Faraday Trans.* **1995**, *91*, 2369.
(19) Stamm, M.; Schubert, D. W. *Annu. Rev. Mater. Sci.* **1995**, *25*, 325.
(20) Farinha, J. P. S.; Vorobyova, O.; Winnik, M. A. *Macromolecules* **2000**, *33*, 5863.
(21) Cahn, J. W.; Hilliard, J. E. *J. Chem. Phys.* **1958**, *28*, 258.
(22) de Gennes, P. G. *Scaling Concepts in Polymer Physics*; Cornell University: Ithaca, NY, 1979.

(23) de Gennes, P. G. *J. Chem. Phys.* **1980**, *72*, 4756.

(24) Anastasiadis, S. H.; Gancarz, I.; Koberstein, J. T. *Macromolecules* **1988**, *21*, 2980.

(25) Schubert, D. W. *Bestimmung der Grenzflächenbreite zwischen unverträglichen Polymeren mit Neutronenreflexion*; Shaker Verlag: Aachen, Germany, 1996.

(26) Feng, J.; Winnik, M. A. *Macromolecules* **1997**, *30*, 4324.

(27) Pham, H.; Farinha, J. P. S.; Winnik, M. A. *Macromolecules* **2000**, *33*, 5850.

(28) Tang, H.; Freed, K. F. *J. Chem. Phys.* **1991**, *94*, 1572.

(29) Ermoshkin, A. V.; Semenov, A. N. *Macromolecules* **1996**, *29*, 6294.

(30) Broseta, D.; Fredrickson, G. H.; Helfand, E.; Leibler, L. *Macromolecules* **1990**, *23*, 132.

(31) Vorobyova, O.; Winnik, M. A. *Macromolecules* **2001**, *34*, 2298.

(32) James, D. R.; Demmer, D. R. M.; Verral, R. E.; Steer, R. P. *Rev. Sci. Instrum.* **1983**, *54*, 1121.

(33) Martinho, J. M. G.; Egan, L. S.; Winnik, M. A. *J. Anal. Chem.* **1987**, *59*, 861.

(34) O'Connor, D. V.; Phillips, D. *Time Correlated Single Photon Counting*; Academic Press: London, 1984.

(35) In the single photon counting literature, the mean square errors of weighted regressions similar to those based on eq 22 are usually denoted by "χ^2"; but here we wish to reserve the "χ" symbol for the Flory−Huggins interaction parameter.

(36) Paul, D. R. *Pure Appl. Chem.* **1995**, *67*, 977.

(37) Paul, D. R.; Barlow, J. W. *Polymer* **1984**, *25*, 487.

(38) Using the group additivity method described in Coleman et. al. (Coleman, M. M.; Serman, C. J.; Bhagwagar, D. E.; Painter, P. C. *Polymer* **1990**, *31*, 1187), we calculate values of $\delta_{PBMA} = 8.67$ cal$^{0.5}$/cm$^{1.5}$ and $\delta_{PEHMA} = 8.30$ cal$^{0.5}$/cm$^{1.5}$.

(39) *Handbook of Chemistry and Physics*, 81st ed.; Lide, D. R., Editor-in-Chief; CRC Press: Boca Raton, FL, 2000−2001.

(40) Olabisi, O.; Simha, R. *Macromolecules* **1975**, *8*, 206.

(41) Van Krevelen, D. W. *Properties of Polymers*; Elsevier: Amsterdam, 1990; p 87.

(42) Simha, R.; Boyer, R. F. *J. Chem. Phys.* **1962**, *37*, 1003.

(43) Mark, H. F.; Bikales, N. M.; Overberger, C. G.; Menges, G. *Encyclopedia of Polymer Science and Engineering*; John Wiley and Sons: New York, 1985; Vol. 1.

(44) Brandrup, J., Immergut, E. H., Grulke, E. A., Eds.; *Polymer Handbook*, 4th ed.; JohnWiley & Sons: New York, 1999; pp VII/50 and VII/51.

(45) Chinai, S. N.; Guzzi, R. A. *J. Polym. Sci.* **1956**, *21*, 417.

(46) Helfand, E.; Sapse, A. M. *J. Chem. Phys.* **1975**, *62*, 1327.

(47) *The Numerical Algorithms Group Limited*; NAG Fortran Library, Mark 15: Oxford, U.K., 1991.